View metadata, citation and similar papers at core.ac.uk

brought to you by CORE

provided by NASA Technical Reports Server

NASA
TP
1952
c.1

NASA
Technical
Paper
1952

December 1981

TECH LIBRARY KAFB, NM
006742

Force and Moment, Flow-Visualization, and Boundary-Layer Tests on a Shuttle Orbiter Model at Mach 6

Robert L. Calloway

LEAN COPY: RETURN TO
AFWL TECHNICAL LIBRARY
KIRTLAND AFB, N.M.

NASA

TECH LIBRARY KAFB, NM

0067642

NASA Technical Paper 1952

1981

Force and Moment, Flow-Visualization, and Boundary-Layer Tests on a Shuttle Orbiter Model at Mach 6

Robert L. Calloway
Langley Research Center
Hampton, Virginia

National Aeronautics and Space Administration

Scientific and Technical Information Branch

The use of trade names in this publication does not constitute endorsement, either expressed or implied, by the National Aeronautics and Space Administration.

C_N normal-force coefficient, $\frac{\text{Normal force}}{q_\infty S}$

$\bar{c}$ mean aerodynamic chord of model wing, m (see table I)

E_{rms} root-mean-square voltage

ℓ model reference length, m (see table I)

M_∞ free-stream Mach number

p_b measured base pressure, kPa

p_t stagnation pressure, kPa

p_∞ free-stream static pressure, kPa

q_∞ free-stream dynamic pressure, kPa

R unit free-stream Reynolds number, m^{-1}

R_ℓ free-stream Reynolds number, based on reference length

S model reference area, m^2 (see table I)

S_b model base area, m^2

T_t stagnation temperature, K

α angle of attack, deg

β angle of sideslip, deg

δ_e elevon deflection angle $\frac{\delta_{e,L} + \delta_{e,R}}{2}$, positive for trailing edge down, deg

δ_{BF} body-flap deflection angle, positive for trailing edge down, deg

Abbreviations:

FRL fuselage reference line

IML inner mold line

OML outer mold line

OMS orbital maneuver system

L left

R right

FACILITY AND TEST CONDITONS

All tests were conducted in the Langley 20-Inch Mach 6 Tunnel, which is an intermittent cycle, blowdown-type facility. The test Mach number was achieved with a fixed-geometry, two-dimensional, contoured nozzle which incorporates a 20.5- by 20.0-inch test section. The model support system has an injection capability with an angle-of-attack range from -5° to 55°, and an angle-of-sideslip range from 0° to -10°. The tunnel air is heated by electrical resistance heaters and exhausts through a movable second minimum into vacuum spheres or into the atmosphere with the aid of an annular air ejector. The ranges of the tunnel operating conditions are as follows:

Stagnation pressure	207 to 3619 kPa (30 to 525 psi)
Stagnation temperature	450 to 566 K (810 to 1018°R)
Reynolds number	2.3×10^6 m^{-1} to 29.5×10^6 m^{-1} (0.7×10^6 ft^{-1} to 9×10^6 ft^{-1})
Dynamic pressure	5.5 to 60 kPa (0.8 to 8.7 psia)

Maximum run time with

1 vacuum sphere	1 minute
2 vacuum spheres	1.5 minutes
The ejector	20 minutes

Operation, flow conditions, and details of force testing in this facility are presented in reference 2. During the force tests, the facility was operated at the following conditions:

M_∞	p_t		T_t		R, m^{-1}	R, ft^{-1}	$R_\ell \times 10^6$
	kPa	psia	K	°R			
5.9	345	50	456	820	2.95×10^6	0.9×10^6	0.4
6.0	1724	250	483	870	14.4	4.4	1.9
6.0	3447	500	500	900	27.6	8.4	3.6

MODELS

All force tests were conducted using a stainless steel 0.004-scale model of the modified 140-C Orbiter configuration (ref. 3), which is designated as model 74-0 (fig. 1). The various model components as defined by Rockwell International are shown in figure 2 and are listed as follows:

B_{62}	fuselage
C_{12}	canopy
W_{127}	wing
E_{43}	elevons
F_{10}	body flap

Three different balances were used to obtain the force-test data to insure accuracy for the three different Reynolds numbers. The following table lists the balances used for each Reynolds number and the data uncertainties (based on ∓0.5 percent of balance design loads) which correspond to each case:

R, m^{-1}	q_∞, kPa	Balance	Uncertainties
2.95×10^6	5.5	HN06	ΔC_N ... ∓0.010 ΔC_A ... ∓0.005 ΔC_m ... ∓0.005
		2039	ΔC_N ... ∓0.040 ΔC_A ... ∓0.003 ΔC_m ... ∓0.016
14.4	27.6	2039	ΔC_N ... ∓0.008 ΔC_A ... ∓0.0006 ΔC_m ... ∓0.003
		2040	ΔC_N ... ∓0.020 ΔC_A ... ∓0.002 ΔC_m ... ∓0.006
27.6	55.2	2040	ΔC_N ... ∓0.010 ΔC_A ... ∓0.001 ΔC_m ... ∓0.003

Data were obtained at the following four Orbiter-model control-surface deflections for all Reynolds numbers:

δ_e, deg	δ_{BF}, deg
-40	-11.7
0	0
10	16.3
0	22.5

Flow Diagnostics

Schlieren photographs were taken to provide flow visualization for each angle of attack, control deflection, and flow condition for both the force tests and the boundary-layer state tests.

The technique and equipment for the hot-film-sensor boundary-layer tests were essentially identical to those used in reference 4 for supersonic speeds. The sensors were operated in a constant temperature mode with an overheat ratio of approximately 1.4. A switch assembly was used to connect each sensor to a single-channel anemometer system, and the bridge-voltage output fluctuation of the system was measured by using a root-mean-square (rms) voltmeter. When a sensor is heated by a constant temperature anemometer device, the sensitivity diminishes as Mach number is increased because of the associated higher temperature levels in the flow. As the

local temperature approaches the temperature limit of the sensor, the corresponding change in voltage required to keep the sensor at a constant temperature is small and is difficult to measure. The sensors, which were designed not to exceed 673 K, were operated at 648 K.

RESULTS AND DISCUSSION

The results of the force tests are presented in figure 7. There is little effect of Reynolds number on C_N or C_m for $\delta_e = -40°$ and $\delta_{BF} = -11.7°$ as shown in figure 7(a). The decrease in axial-force coefficient with increasing Reynolds number follows the expected trend. For the control deflection of $\delta_e = \delta_{BF} = 0°$ (fig. 7(b)), similar trends are noted, except for a slightly higher increase in C_A with increase in angle of attack for the highest Reynolds number case.

Data from Tunnel "B" at Arnold Engineering Development Center (AEDC) (ref. 5) are compared with the present results for $\delta_e = 10°$ and $\delta_{BF} = 16.3°$ in figure 7(c). Note that the present results agree with the axial-force coefficients measured at AEDC for nonmatching Reynolds numbers and that the present data have a more positive (nose-up) pitching moment over the entire α range for all three Reynolds numbers. The axial-force results indicate that the data might be matched from the two facilities by adjusting the unit Reynolds numbers to match the local transition Reynolds number as suggested by Pate (ref. 1). The pitching-moment data do not support this supposition; in fact, the pitching-moment data do not appear to be Reynolds number dependent. A check on the accuracy of the data measurement at AEDC indicates that these values are at least as good as the present data. Perhaps small differences in model fidelity and known model differences can account for the disagreement.

The highest Reynolds number axial-force data from the present test show an unusual trend. There is a significant increase or "jump" in the axial-force coefficient between 25° and 30°. Although there is no comparison with other data for $\delta_e = 0°$ and $\delta_{BF} = 22.5°$ (fig. 7(d)), the same trend occurs in the axial-force coefficient as was shown for $\delta_e = 10°$ and $\delta_{BF} = 16.3°$. This measured phenomenon in axial-force coefficient is either only present for, or is magnified by, the positive control deflections (see figs. 7(a) and 7(b)).

The schlieren photographs, which were taken simultaneously with the force-test data, were studied carefully to determine a cause for the C_A trend with α for the highest Reynolds number and positively deflected control surfaces. These studies revealed that as the Reynolds number changed, definite differences in the shock structure in the vicinity of the body flap were apparent. The differences in the shock structure are shown in figure 8 for $\delta_e = 0°$ and $\delta_{BF} = 22.5°$. This figure is a collection of close-ups of the body-flap region for all the angles of attack and all three test Reynolds numbers. Note that for $R_\ell = 0.4 \times 10^6$ and 1.9×10^6, the shock from the body flap does not change significantly as α varies from 20° to 40°. However, for $R_\ell = 3.6 \times 10^6$ there is a significant change in the shock wave ahead of the body flap as the angle of attack changes from 25° to 30°. For $\alpha = 30°$ to 40°, this shock wave moves forward and farther away from the flap. This observation, plus an apparent change in the character of the local flow field (as indicated by the change in the extent of the separation region, the boundary-layer thickness, and apparent turbulence) provided justification for the hot-film-sensor tests, which could determine conclusively the state of the windward boundary layer.

Initially, the hot-film tests were conducted in the same manner as the force tests, that is, injecting the model and recording the data at a constant Reynolds number while changing the angle of attack. This method, while it most closely matched the model-wall temperature of the force tests, was not satisfactory because the transition location was very sensitive to small changes in angle of attack, and thus was hard to determine. Another method was used whereby the model was injected at the desired angle of attack and then the Reynolds number was increased in a stepwise fashion while the output of the sensors was recorded. Figure 9 presents data obtained from the #2 sensor only, which was located near the middle of the model. Although not presented, all the data from the forward sensor (#1) indicated a laminar boundary layer, whereas the data from the rearward sensor (#3) are suspect, since its output was irregular throughout the testing period. The location of transition (as determined by sensor #2) is indicated quite clearly in figure 9. As the angle of attack increased from 30° to 40°, the onset of transition occurred at unit Reynolds numbers of approximately 24×10^6 to 16×10^6 per meter, respectively. This Reynolds number range corresponds to length Reynolds numbers of 3.2×10^6 to 2.1×10^6 which includes the highest case for the force tests as indicated by the C_A values plotted at the top of figure 9. The arrows and bars are included to show how the rms voltage changed as the transition location moved with wall temperature or perhaps small changes in the tunnel unit Reynolds number. They also give the reader an indication of the dynamic character of the voltage reading as it was used to determine the boundary-layer state. The results of the hot-film-sensor tests, as presented in figure 9, clearly show that the rearward portion of the force-test model had a turbulent windward boundary layer for angles of attack of 30° and above for $R_\ell = 3.6 \times 10^6$.

CONCLUDING REMARKS

Results from force and moment, flow-visualization, and boundary-layer state tests which were conducted in the Langley 20-Inch Mach 6 Tunnel using two 0.004-scale Shuttle Orbiter models are presented. The force and moment tests were conducted for an angle-of-attack range from 20° to 40° and for Reynolds numbers based on reference length from 0.4×10^6 to 3.6×10^6. Schlieren photographs were obtained for each angle of attack and Reynolds number. The boundary-layer state tests, which were conducted using hot-film sensors mounted in a separate model, were conducted over the same range of conditions as the force tests.

Test results were combined to show that changes in the boundary layer on a typical hypersonic force-test model can affect the aerodynamic characteristics. The local flow on the windward side changed from laminar to transitional to turbulent as the angle of attack increased and/or the Reynolds number increased, which proved that the aft control surfaces encountered turbulent flow for these conditions during the force tests.

This study has shown that hot-film-sensor tests can be used in hypersonic test facilities to determine the state of the local boundary-layer flow. One or two sensors mounted toward the rear of a force-test model can provide critical information (with no interference effects) during a force test without conducting a separate, independent, flow assessment. Information about the state of the local boundary layer, as determined by these sensors, is especially important for hypersonic aero-

dynamic testing on vehicles which operate at high angles of attack with aft control surfaces and for studies which compare results for a range of model sizes, facilities, and test conditions.

Langley Research Center
National Aeronautics and Space Administration
Hampton, VA 23665
October 23, 1981

REFERENCES

1. Pate, Samuel Ralph: Dominance of Radiated Aerodynamic Noise on Boundary-Layer Transition in Supersonic-Hypersonic Wind Tunnels: Theory and Application. Ph. D. Thesis, Univ. of Tennessee, 1977.

2. Keyes, J. Wayne: Force Testing Manual for the Langley 20-Inch Mach 6 Tunnel. NASA TM-74026, 1977.

3. Hawthorne, P. J.: Results of Investigations on an 0.004-Scale 140C Modified Configuration Space Shuttle Vehicle Orbiter Model (74-0) in the NASA/Langley Research Center Hypersonic Nitrogen Tunnel (0A89). NASA CR-141, 513, 1975.

4. Stallings, Robert L., Jr.; and Lamb, Milton: Effects of Roughness Size on the Position of Boundary-Layer Transition and on the Aerodynamic Characteristics of a 55° Swept Delta Wing at Supersonic Speeds. NASA TP-1027, 1977.

5. Gillins, R. L.: Results of Investigations (0A77 and 0A78) on an 0.015-Scale 140A/B Configuration Space Shuttle Vehicle Orbiter Model 49-0 in the AEDC VKF B and C Wind Tunnels. NASA CR-134, 429, Revision A, 1975.

TABLE I.- FULL-SCALE GEOMETRIC CHARACTERISTICS OF THE

140-C SPACE SHUTTLE ORBITER

Body, B_{62}:	
Length (measured from OML), m (in.)	32.850 (1293.3)
Length (measured from IML), m (in.)[a]	32.774 (1290.3)
Maximum width, m (in.)	6.706 (264.0)
Maximum depth, m (in.)	6.350 (250.0)
Fineness ratio	4.899
Canopy, C_{12}:	
Length, m (in.)	3.641 (143.357)
Maximum width, m (in.)	3.871 (152.412)
Maximum depth, m (in.)	1.311 (51.61)
Wing, W_{127}:	
Planform area (theoretical), m^2 (ft^2)[a]	249.910 (2690.00)
Span, m (in.)[a]	23.792 (936.68)
Aspect ratio	2.265
Dihedral angle, deg	3.500
Incidence angle, deg	0.500
Sweepback angle (leading edge), deg	45.000
Sweepback angle (trailing edge), deg	-10.056
Aerodynamic twist, deg	3.000
Mean aerodynamic chord, m (in.)[a]	12.060 (474.81)
Root chord (theoretical), m (in.)	17.507 (689.24)
Tip chord (theoretical), m (in.)	3.501 (137.85)
Airfoil section at root	Modified NACA 0011.3-64
Airfoil section at tip	Modified NACA 0012-64
Elevon, E_{43} (for one side):	
Planform area, m^2 (ft^2)	19.510 (210.0)
Span (equivalent), m (in.)	8.870 (349.2)
Inboard chord (equivalent), m (in.)	2.997 (118.004)
Outboard chord (equivalent), m (in.)	1.402 (55.192)
Sweepback angle at leading edge, deg	0.00
Sweepback angle at trailing edge, deg	-10.056

[a]Reference values.

TABLE I.- Concluded

Body flap, F_{10}:

Planform area, m^2 (ft^2)	12.542 (135.00)
Maximum width, m (in.)	6.502 (256.00)
Maximum depth, m (in.)	0.503 (19.798)
Length, m (in.)	2.223 (87.50)

Vertical tail, V_8:

Planform area (theoretical), m^2 (ft^2)	38.393 (413.253)
Span (theoretical), m (in.)	8.019 (315.72)
Aspect ratio	1.675
Sweepback angle at leading edge, deg	45.000
Sweepback angle at trailing edge, deg	26.2
Root chord (theoretical), m (in.)	6.821 (268.50)
Tip chord (theoretical), m (in.)	2.755 (108.47)
Airfoil section -	
Leading wedge angle, deg	10.000
Trailing wedge angle, deg	14.92

Rudder, R_5:

Area, m^2 (ft^2)	9.304 (100.15)
Span (equivalent), m (in.)	5.105 (201.00)
Inboard chord, m (in.)	2.326 (91.585)
Outboard chord, m (in.)	1.291 (50.833)
Sweepback angle at hinge line, deg	34.83
Sweepback angle at trailing edge, deg	26.25

OMS pod, M_{14}:

Length, m (in.)	6.452 (254.0)
Maximum width, m (in.)	3.444 (135.6)
Maximum depth, m (in.)	1.869 (73.6)

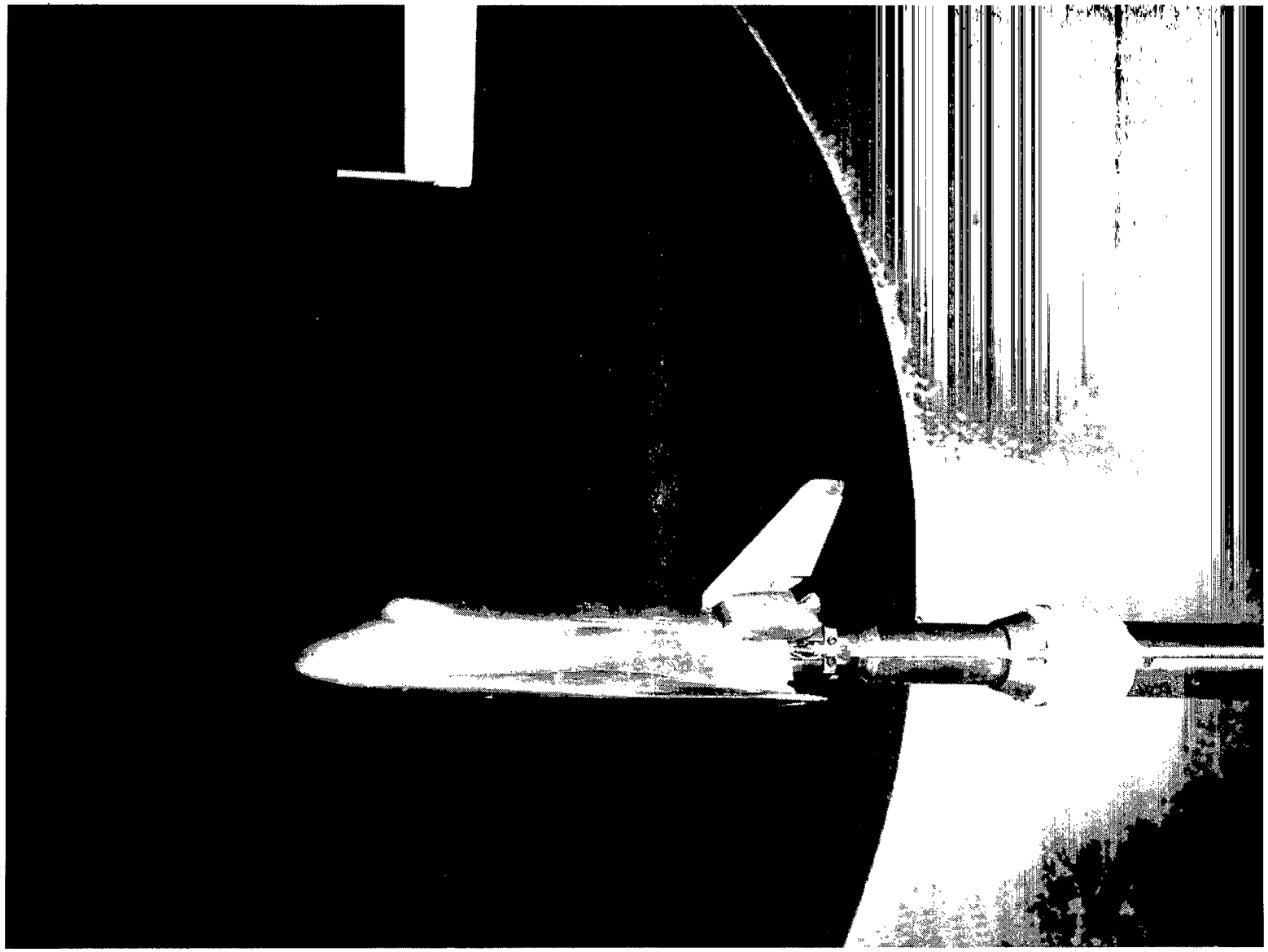

Figure 1.- Photograph of model 74-0 as tested.

L-77-4566

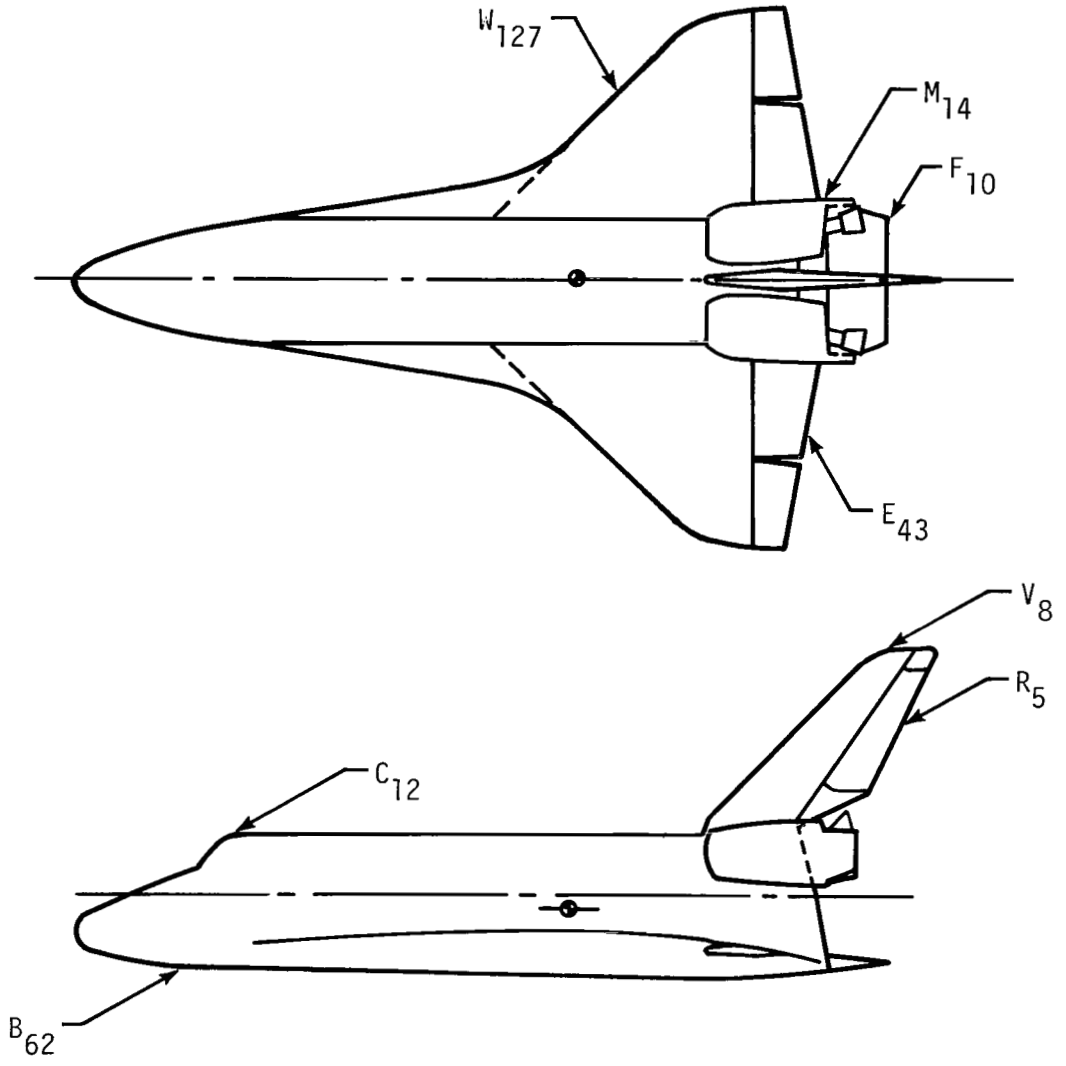

Figure 2.- Designations of force-test model components.

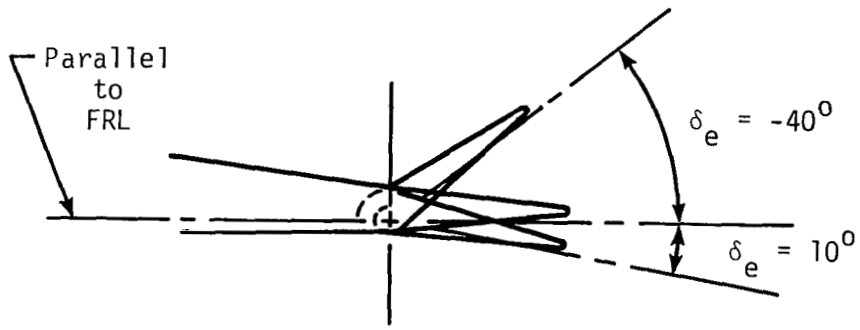

Elevon deflections

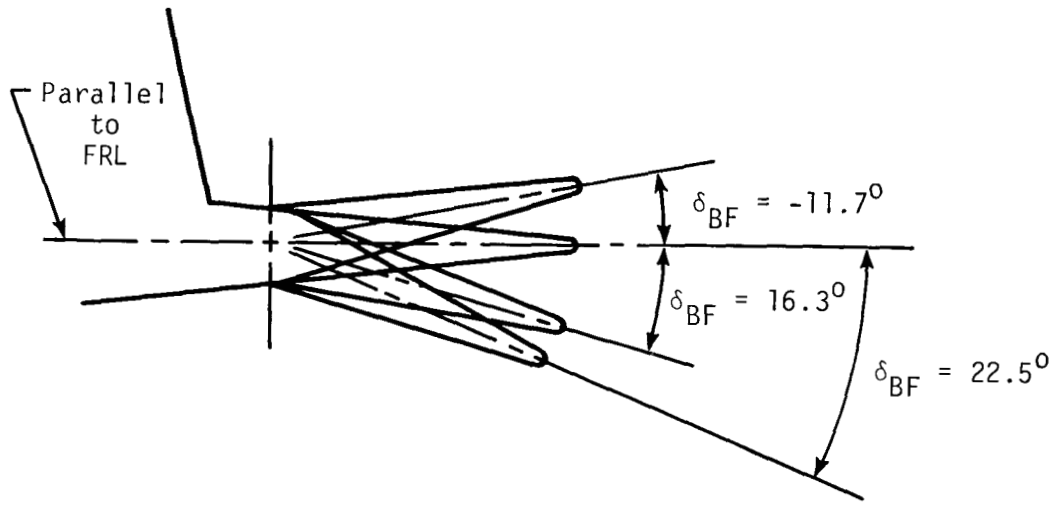

Body-flap deflections

Figure 3.- Definition of the elevon and body-flap deflections.

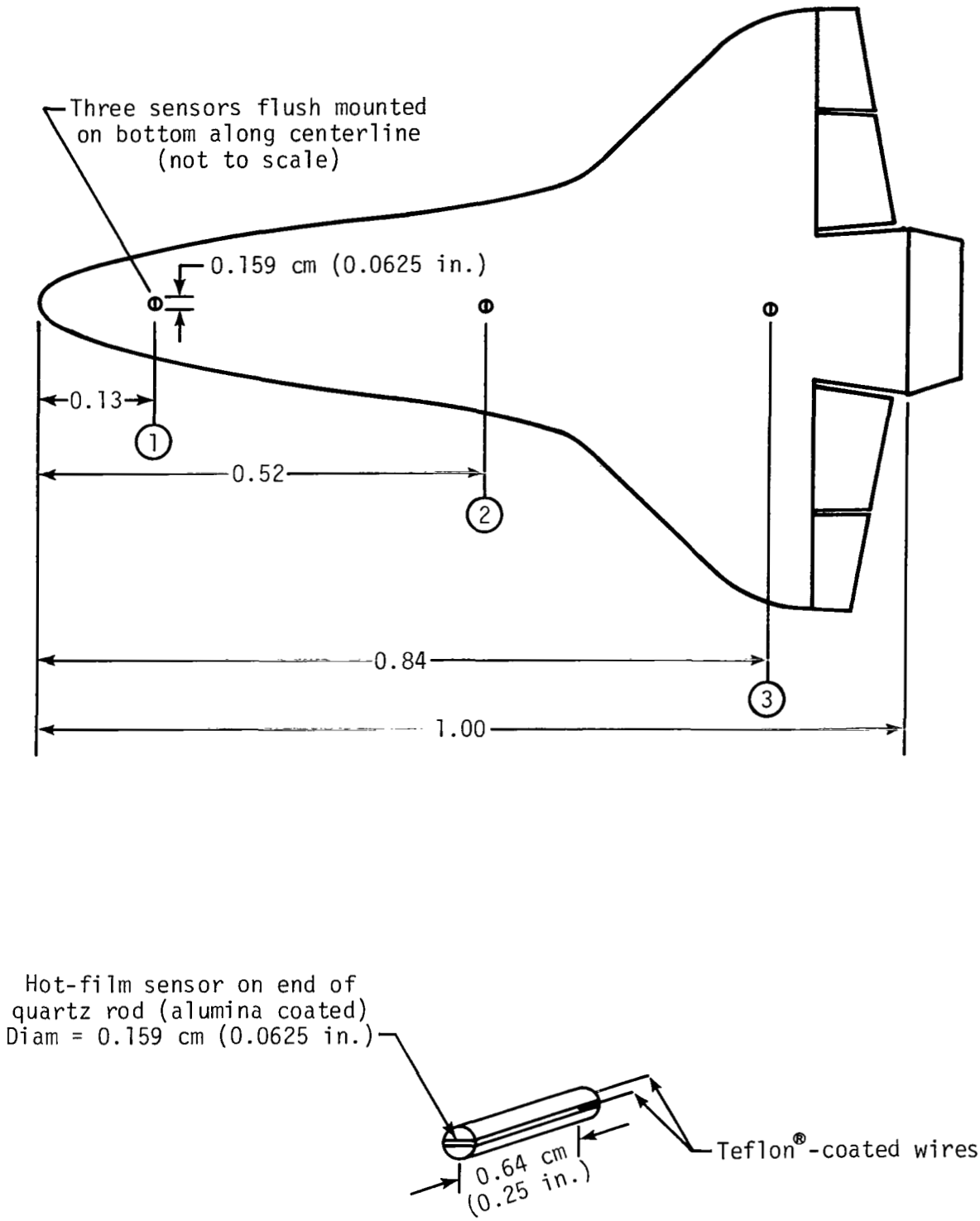

Figure 4.- Sketch of hot-film sensor and locations on bottom of model. Dimensions are normalized by reference length ℓ.

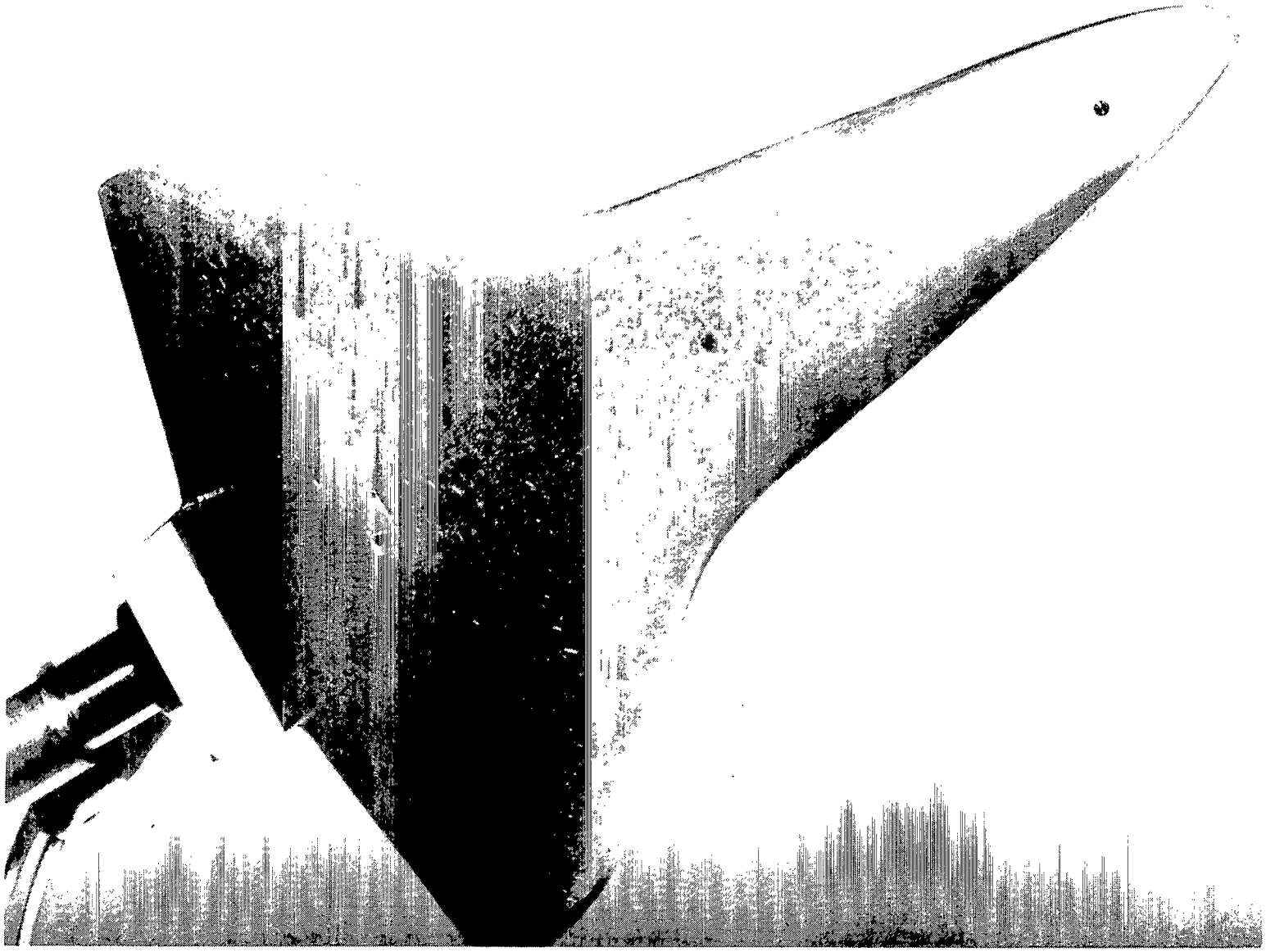

L-79-7809

(a) Bottom view.

Figure 5.- Photograph of hot-film-sensor model as tested.

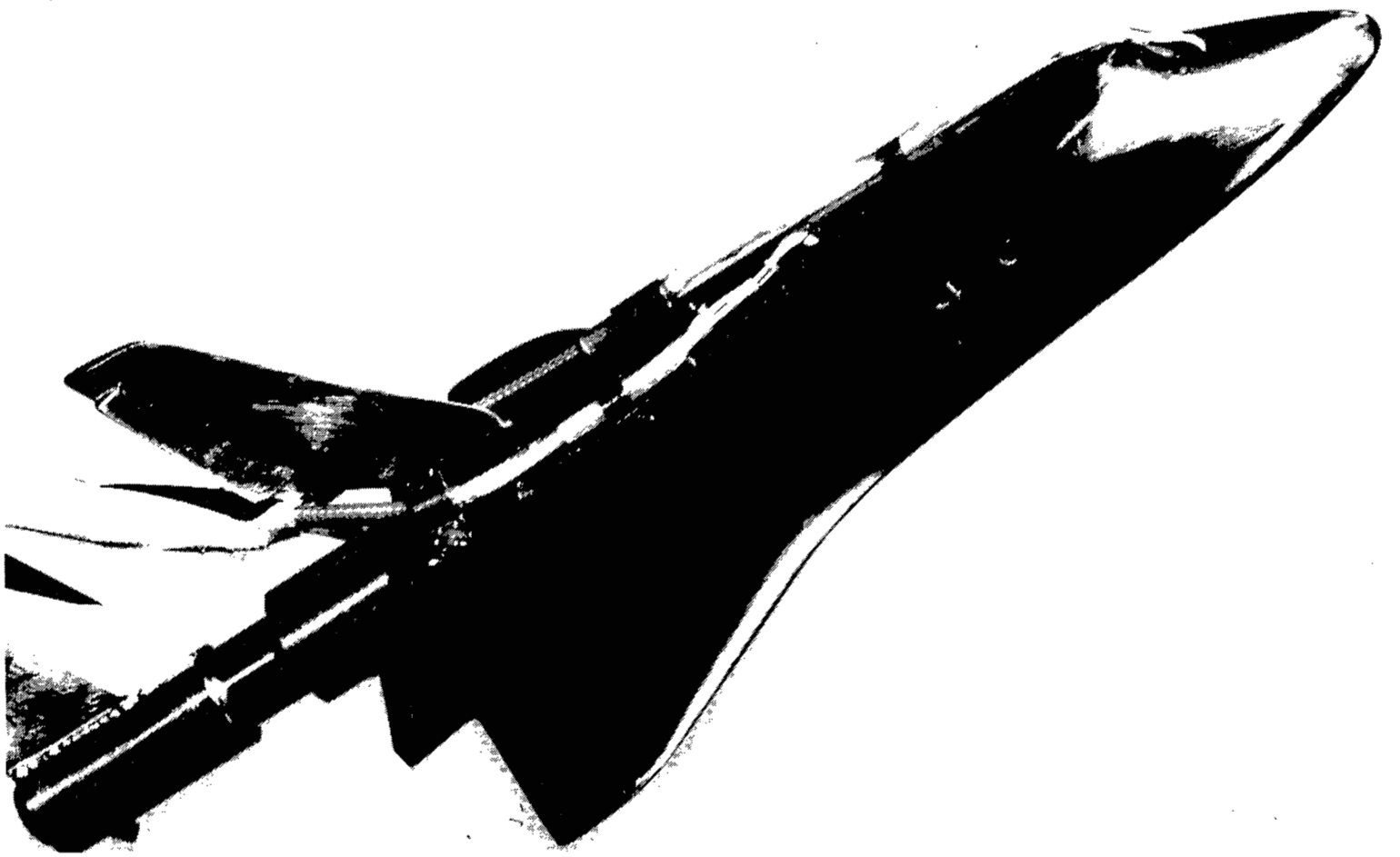

(b) Side and top view.

L-79-7811

Figure 5.- Concluded.

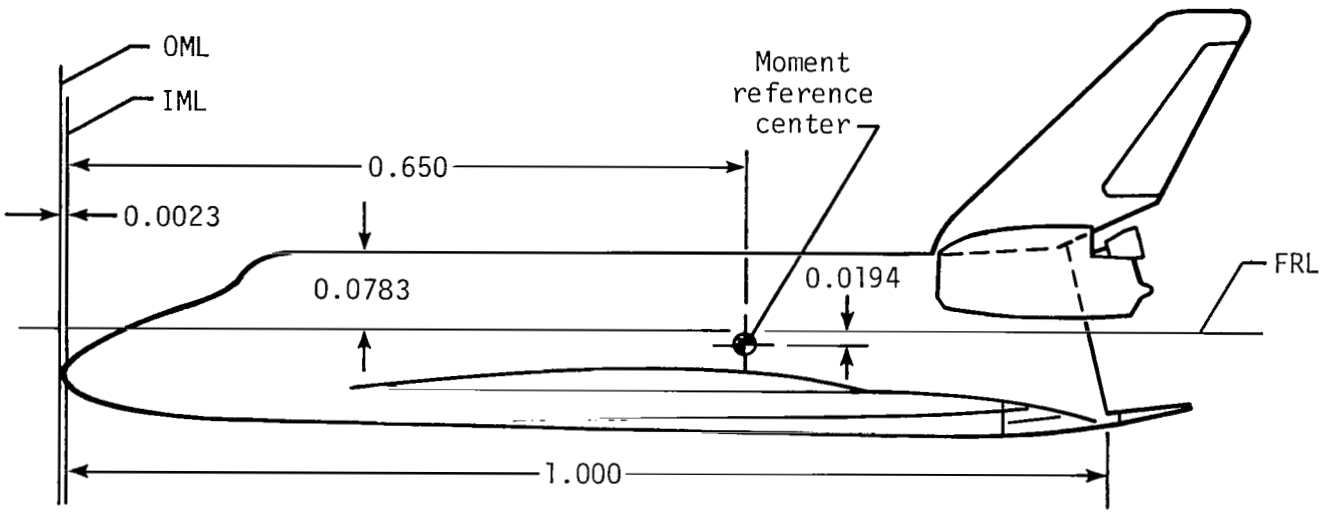

(a) Moment reference dimensions, normalized by reference length ℓ.

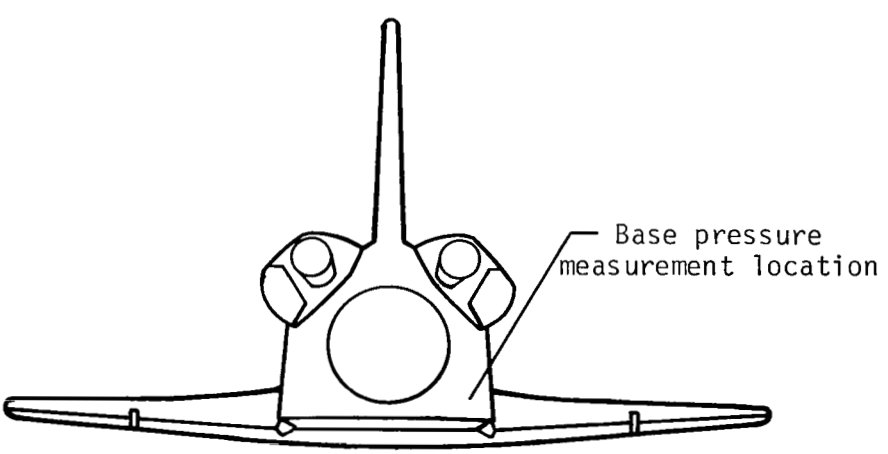

(b) Rear view.

Figure 6.- Sketch of force-test model.

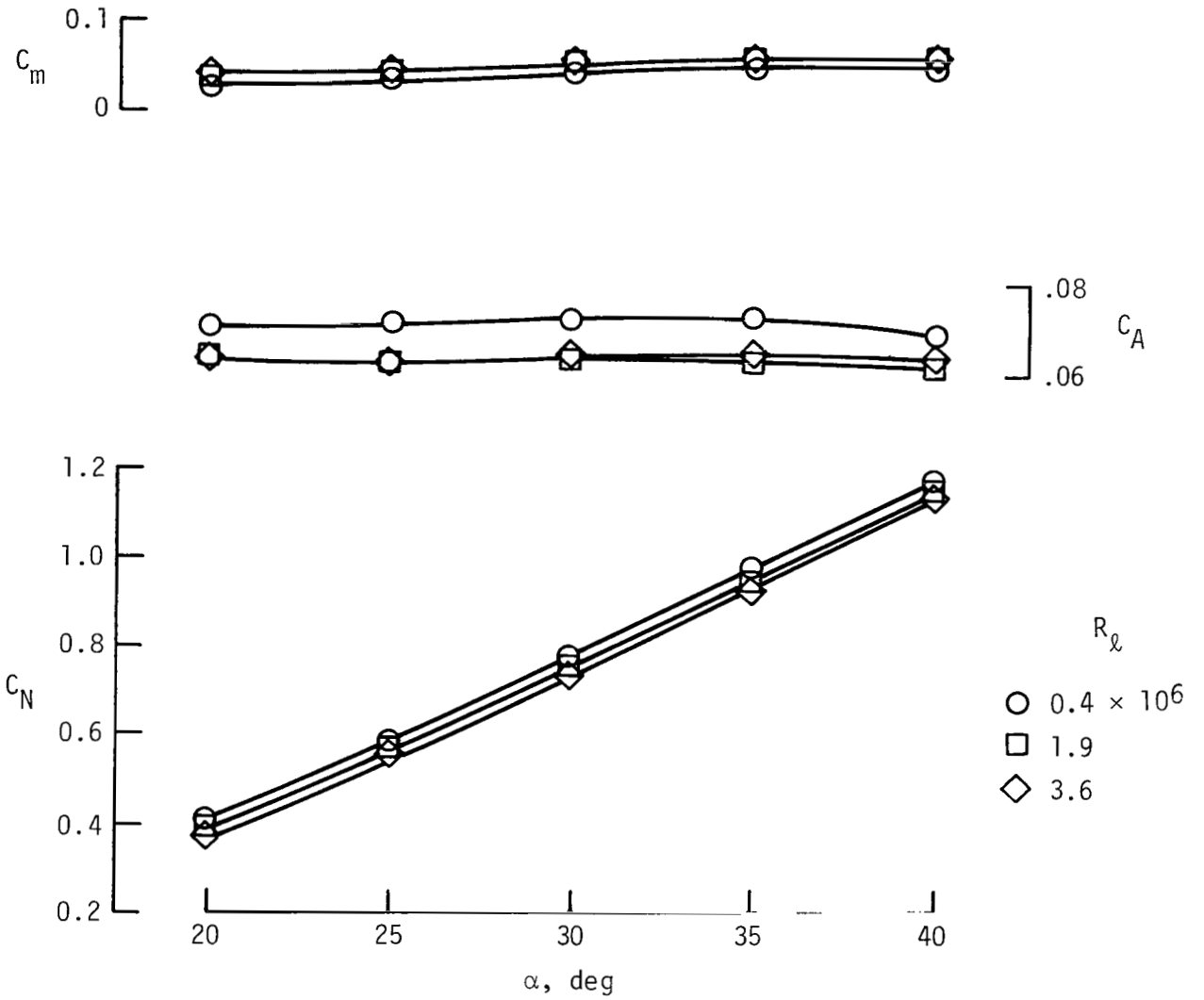

(a) $\delta_e = -40°$; $\delta_{BF} = -11.7°$.

Figure 7.- Effect of Reynolds number on the static longitudinal aerodynamic coefficients.

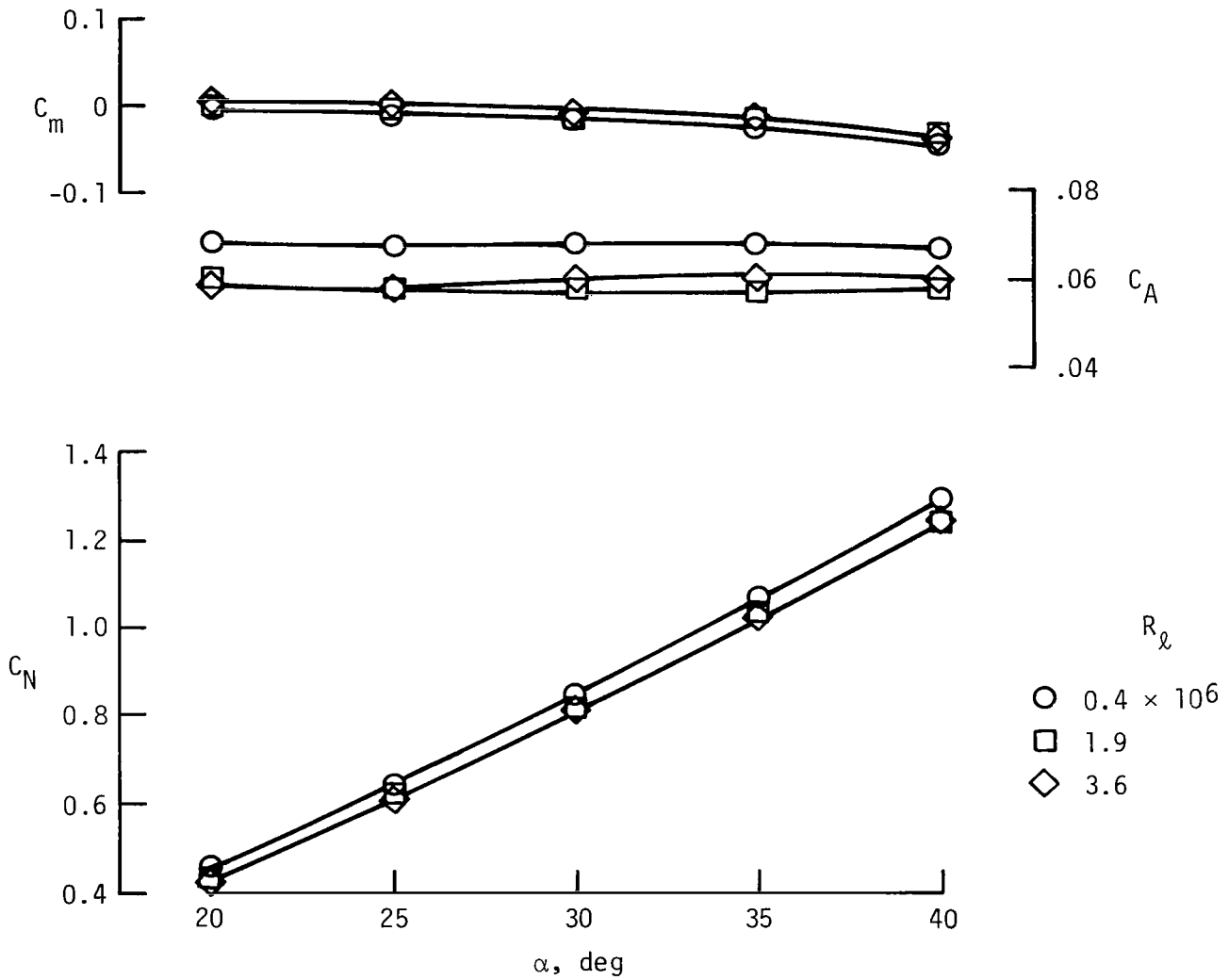

(b) $\delta_e = 0°$; $\delta_{BF} = 0°$.

Figure 7.- Continued.

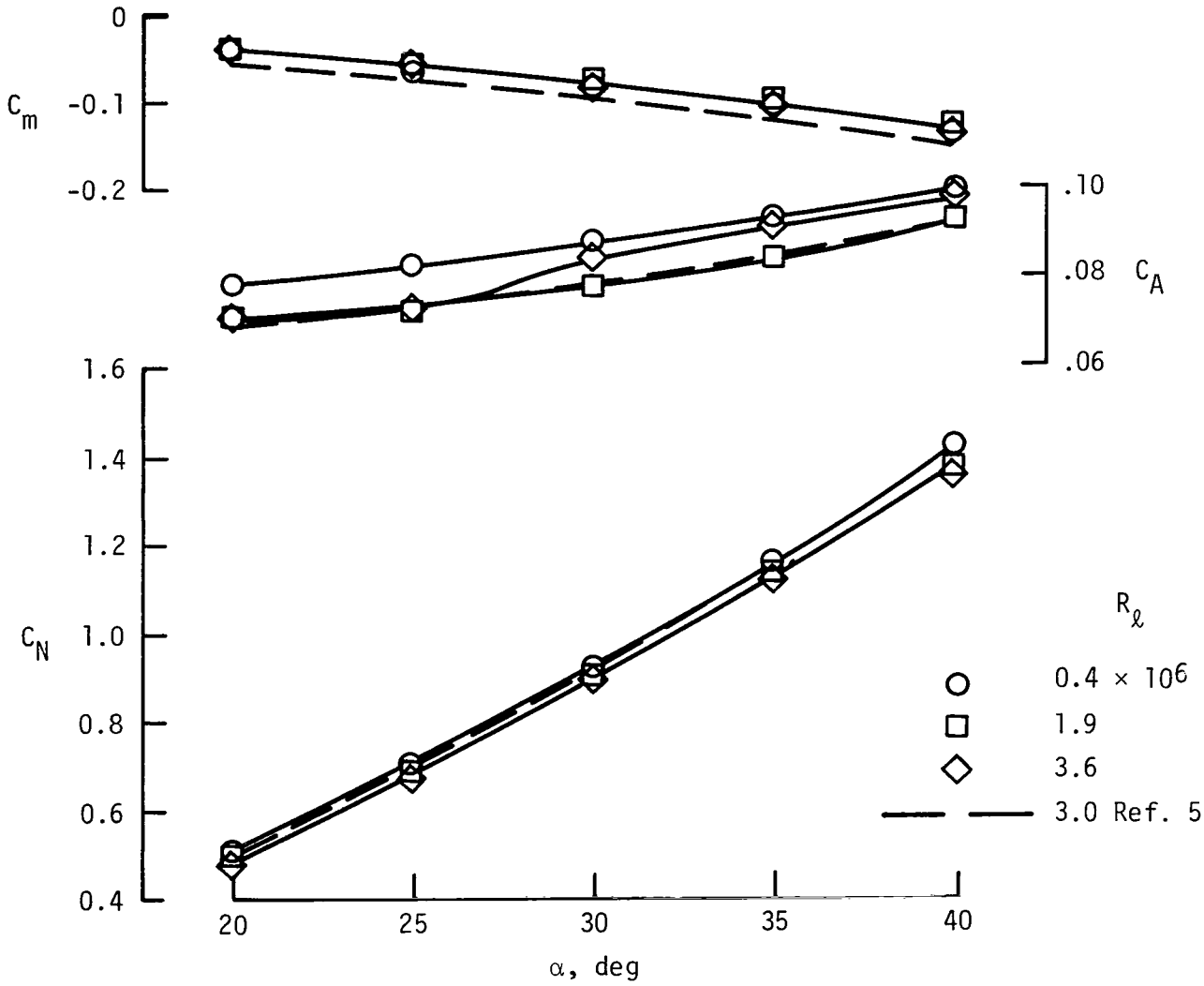

(c) $\delta_e = 10°$; $\delta_{BF} = 16.3°$.

Figure 7.- Continued.

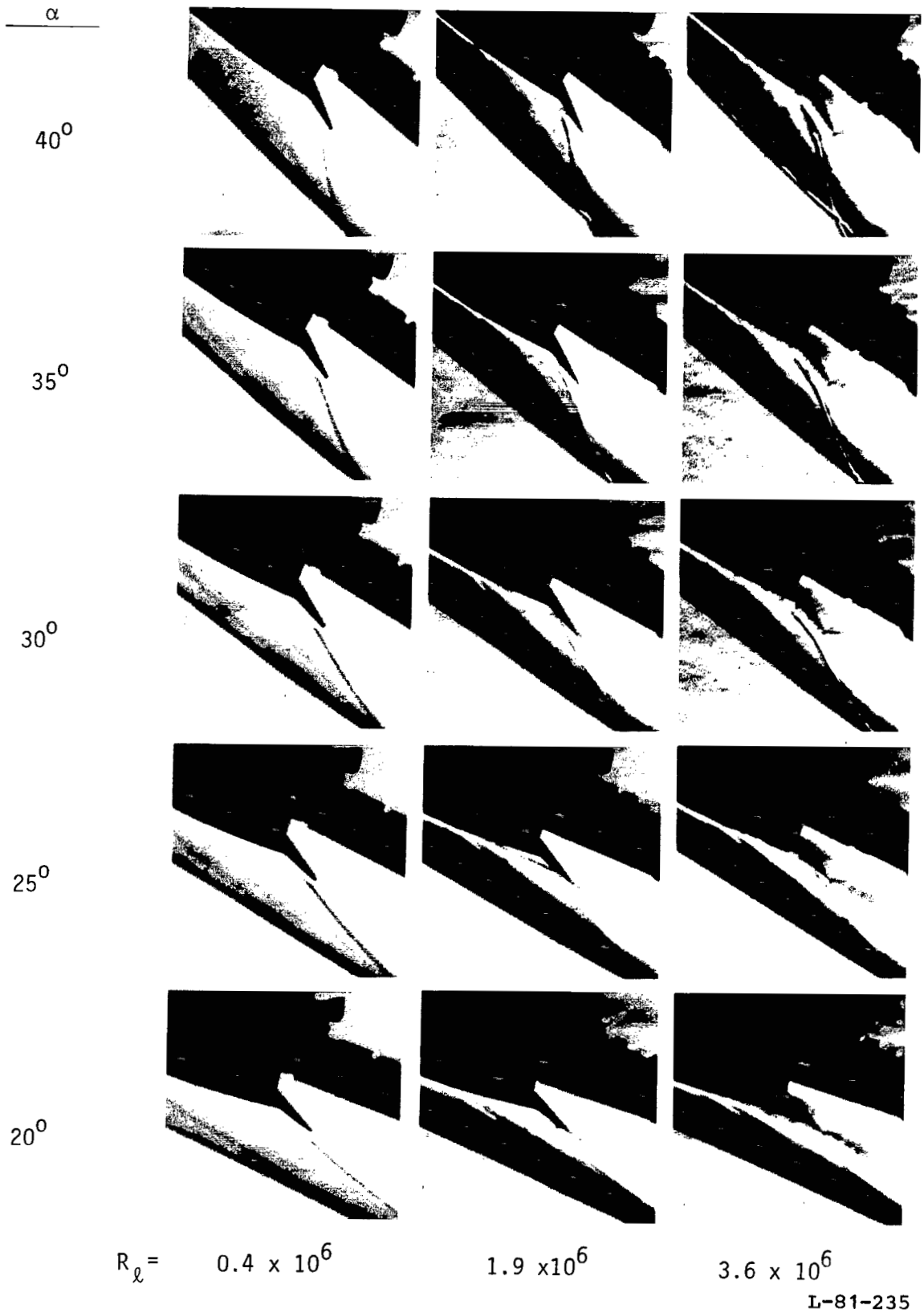

Figure 8.- Close-up of body-flap region from schlieren photographs. $\delta_e = 0°$; $\delta_{BF} = 22.5°$.

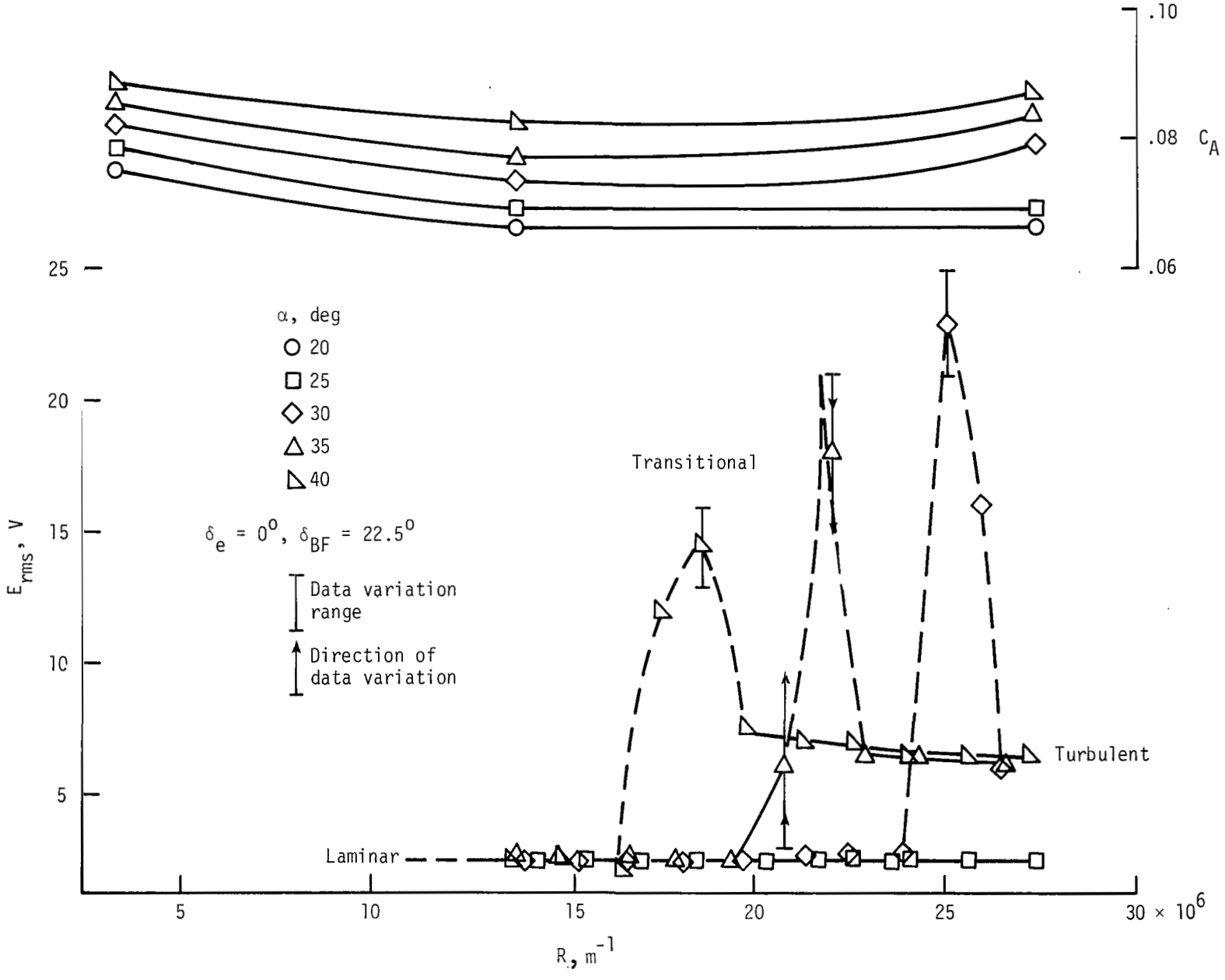

Figure 9.- Effect of Reynolds number and angle of attack on transition and C_A as measured by sensor #2.

1. Report No.	2. Government Accession No.	3. Recipient's Catalog No.
NASA TP-1952		

4. Title and Subtitle

FORCE AND MOMENT, FLOW-VISUALIZATION, AND BOUNDARY-LAYER TESTS ON A SHUTTLE ORBITER MODEL AT MACH 6

5. Report Date: December 1981

6. Performing Organization Code: 506-51-13-02

7. Author(s)

Robert L. Calloway

8. Performing Organization Report No.: L-14782

10. Work Unit No.:

9. Performing Organization Name and Address

NASA Langley Research Center
Hampton, VA 23665

11. Contract or Grant No.:

13. Type of Report and Period Covered: Technical Paper

12. Sponsoring Agency Name and Address

National Aeronautics and Space Administration
Washington, DC 20546

14. Sponsoring Agency Code:

15. Supplementary Notes

16. Abstract

Results from force and moment, flow-visualization, and boundary-layer state tests which were conducted in the Langley 20-Inch Mach 6 Tunnel using two 0.004-scale Shuttle Orbiter models are presented. The force and moment tests were conducted for an angle-of-attack range from 20° to 40° and for Reynolds numbers based on reference length from 0.4×10^6 to 3.6×10^6. Schlieren photographs were obtained for each angle of attack and Reynolds number. The boundary-layer state tests, which were conducted using hot-film sensors mounted in a separate model, were conducted over the same range of conditions as the force tests. Test results were combined to show that changes in the boundary layer on a typical hypersonic force-test model can affect measurement of the axial-force coefficient and that information about the state of the local boundary layer is important for interpreting hypersonic aerodynamic test results.

17. Key Words (Suggested by Author(s))

Space transportation
Hypersonic aerodynamics
Boundary-layer transition

18. Distribution Statement

Unclassified - Unlimited

Subject Category 02

19. Security Classif. (of this report)	20. Security Classif. (of this page)	21. No. of Pages	22. Price
Unclassified	Unclassified	24	A02

For sale by the National Technical Information Service, Springfield, Virginia 22161

NASA-Langley, 1981

National Aeronautics and
Space Administration

Washington, D.C.
20546

Official Business
Penalty for Private Use, $300

THIRD-CLASS BULK RATE

Postage and Fees Paid
National Aeronautics and
Space Administration
NASA-451

U.S.MAIL

S 1 1U,A, 112581 30090303
DEPT OF THE AIR FORCE
AF WEAPONS LABORATORY
ATTN: TECHNICAL LIBRARY (SUL)
KIRTLAND AFB NM 87117

NASA

POSTMASTER: If Undeliverable (Section 158 Postal Manual) Do Not Return